Journal of Power Sources 203 (2012) 233–242

Contents lists available at SciVerse ScienceDirect

Journal of Power Sources

journal homepage: www.elsevier.com/locate/jpowsour

Supercapacitive behavior and high cycle stability of todorokite-type manganese oxide with large tunnels

Zhenjie Sun[a], Hongyu Chen[a,b,d], Dong Shu[a,b,d,*], Chun He[c,*], Shaoqing Tang[a], Jie Zhang[a]

[a] School of Chemistry and Environment, South China Normal University, Guangzhou 510006, PR China
[b] Base of Production, Education & Research on Energy Storage and Power Battery of Guangdong Higher Education Institutes, Guangzhou 510006, PR China
[c] School of Environmental Science and Engineering, Sun Yat-sen University, Guangzhou 510275, PR China
[d] Key Laboratory of Electrochemical Technology on Energy Storage and Power Generation of Guangdong Higher Education Institutes, South China Normal University, Guangzhou 510006, PR China

ARTICLE INFO

Article history:
Received 29 August 2011
Received in revised form
10 November 2011
Accepted 15 November 2011
Available online 23 November 2011

Keywords:
Todorokite
Manganese oxide
Supercapacitor
Cycle stability

ABSTRACT

A todorokite-type manganese oxide (T-MnO_x) with a 3×3 large tunnel structure was successfully synthesized by a hydrothermal method and employed as an active electrode material for a supercapacitor. The todorokite structure of the as-prepared manganese oxide was confirmed by X-ray diffraction (XRD), and the fragmented platelets were observed by scanning electron microscopy (SEM). The electrochemical performances of the as-prepared T-MnO_x were evaluated by cyclic voltammetry (CV), galvanostatic charge–discharge (CD) experiments and electrochemical impedance spectroscopy (EIS) in 1 M Na_2SO_4 electrolyte. The specific capacitance of the T-MnO_x electrode sharply increased during the initial 1000 cycles and then continued improving gradually. It reached a maximum of 220 F g^{-1} at approximately the 4000th cycle at a scan rate of 2 mV s^{-1}, and further studies showed that the morphology and structure of the T-MnO_x were maintained after 4000 cycles, indicating that an electrochemical activation process occurred during the initial thousands of cycles. The electrochemical activation mechanism is discussed in detail. The specific capacitance remained an almost constant value and decreased slightly upon prolonged cycling. After 23,000 cycles, it decreased by 6% of the maximum specific capacitance. The experimental results demonstrate that T-MnO_x is a promising candidate as an electrode material for supercapacitors.

1. Introduction

Currently, the depletion of fossil fuel resources and environmental issues are becoming more and more serious, creating an urgent demand for the development of a new energy storage device to meet present-day power demands. Supercapacitors are considered promising candidates for energy storage owing to their higher energy density compared with conventional electrical double-layer capacitors and greater power density and longer cycle life than secondary batteries [1,2]. Accordingly, they have been employed in a wide range of applications, such as in memory back-up systems, portable electronics and large industrial equipment, particularly in low-emission hybrid electric vehicles (HEVs) and fuel-cell electric vehicles (FCEVs) for power enhancement in short-pulse applications. Thus, these devices have garnered great research interest in recent years [3].

Because the material composition of the electrode is one of the most important factors that determine the properties of supercapacitors, most researchers in this field have focused on the development of new electrode materials with superior electrochemical properties. The electrode materials used in supercapacitors mainly include carbon-based materials, transition metal oxides and conducting polymers. For these three types of electrode materials, carbon-based materials are widely applied in supercapacitors, but they exhibit a limited voltage window and poor specific energy density. Conducting polymers, such as polyaniline, have gained enormous attention as electrode materials in supercapacitors due to their ease of synthesis, excellent environmental stability, relatively high conductivity and high capacitance; but their poor cyclability is one of their main limitations for widespread application [4]. Therefore, transition metal oxides are attracting growing research interest. Among the various transition metal oxides, hydrous ruthenium oxide ($RuO_2 \cdot nH_2O$) shows the best performance; it exhibits a high capacitance of 760 F g^{-1} and an excellent reversibility in sulfuric acid electrolyte [5]. However, the toxic nature and high cost of hydrous ruthenium oxide greatly limit its commercial implementation. At this point, new transition metal oxides are being considered to replace ruthenium oxides.

* Corresponding authors at: School of Chemistry and Environment, South China Normal University, Guangzhou 510006, PR China. Tel.: +86 20 39310212.
E-mail addresses: dshu@scnu.edu.cn (D. Shu), hechun@mail.sysu.edu.cn (C. He).

0378-7753/$ – see front matter © 2011 Elsevier B.V. All rights reserved.
doi:10.1016/j.jpowsour.2011.11.043

Table 1
The specific capacitance of MnO_2 with different characteristic tunnels.

Reference	MnO_2 form	Tunnel	Specific capacitance ($F g^{-1}$)	Scan rate ($mV s^{-1}$)
[8]	β-MnO_2	1×1	5	5
[9]	Pyrolusite	1×1	28	5
[9]	Ramsdellite	1×2	87	5
[10]	Birnessite	$1 \times \infty$	96	5
[11]	Birnessite	$1 \times \infty$	145	2
[12]	α-MnO_2	2×2	165	10
[7]	α-MnO_2	2×2	166	2

Manganese oxides are considered as the most promising transition metal oxide for the next generation of supercapacitors because of their natural abundance, low cost, wide voltage windows, high specific capacitance and environmentally friendly nature.

Since the ideal supercapacitor behavior of amorphous $MnO_2 \cdot nH_2O$ was first reported by Lee and Goodenough in 1999 [6], manganese oxides have attracted more and more attention, and much effort has been devoted to their research. A literature survey reveals that considerable attention has been paid to tunnel-structure manganese oxides most recently. The microstructures of this type of manganese oxide consist of MnO_6 octahedra, which can be linked along their edges and at their corners to form various tunnel structures. Depending on the link mode of the MnO_6 units in the MnO_2 unit cell, different sizes of the tunnels are obtained, such as β-MnO_2 (1×1), ramsdellite (1×2), birnessite ($1 \times \infty$), α-MnO_2 (2×2), as well as others. The corresponding crystallographic structures of these manganese oxides are schematized in Fig. 1. Because the pseudocapacitive contribution of manganese oxides with various tunnels originates from the intercalation or deintercalation of electrolyte cations into their tunnels, the size of the tunnels should significantly influence their ultimate electrochemical capacitive properties. The most recent and relevant literature regarding these materials has been culled and analyzed, and the manganese oxides with different characteristic tunnels in their structures and the corresponding specific capacitance are summarized in Table 1. Notably, Table 1 shows that the specific capacitance increases with an increase in the tunnel size. The issue to address here concerns the impact of the tunnel size on the specific capacitance. A narrow tunnel size does not allow the intercalation of electrolyte cations into the MnO_2 microstructure because the size of the tunnel is smaller than the diameter of the electrolyte cations. The lower capacitance of such structures is only due to surface adsorption. Contrarily, a large tunnel structure is suitable for the insertion/extraction of electrolyte cations. Furthermore, a large tunnel structure can accommodate a large amount of electrolyte cations, which is essential to sustain the capacitance behavior and stability of the electrode [13]. The todorokite-type MnO_2 has a 3×3 large tunnel structure, as shown in Fig. 1e, which is expected to have excellent electrochemical capacitive properties.

Because todorokite-type MnO_2 possesses this especially large tunnel structure and can absorb some metal cations and various kinds of molecules, this material has wide applications, such as molecular sieves, catalysts and cathodic materials for rechargeable batteries [14–16]. However, to the best of our knowledge, there has been very little work reported in the literature on the application of todorokite-type MnO_2 as an electrode for supercapacitors [9]. In this paper, T-MnO_x was synthesized and studied as a possible active electrode material in a supercapacitor. The supercapacitive behaviors and the charge storage mechanism of T-MnO_x as an electrode material for supercapacitors were studied elaborately and are discussed in detail.

2. Experimental

2.1. Material synthesis

T-MnO_x was synthesized following a procedure similar to that discussed in a previous report by Ching et al. [17]. First, 3.4 g of $MnSO_4 \cdot H_2O$ powder was dissolved in 20 mL of distilled water. While the solution was stirring, 30 mL of NaOH (6 M) aqueous solution was slowly dropped into the solution at room temperature, and a light brown slurry of $Mn(OH)_2$ was obtained. After stirring for approximately 1 h, $Mn(OH)_2$ was oxidized by very slowly adding 3.2 g of $(NH_4)_2S_2O_8$ and 0.7 g of $MgSO_4 \cdot 7H_2O$ granular mixture at room temperature, obtaining an olive-green slurry of Mg-doped Na-birnessite. The obtained slurry was stirred for 2 h at room temperature and then filtered and repeatedly washed with distilled water. The Mg-buserite was prepared by dispersing the Mg-doped Na-birnessite in 300 mL of 1 M of $MgCl_2$ solution and stirring for 24 h at room temperature. The resulting mixture was transferred into a Teflon-lined autoclave and kept in an oven at 160 °C for 24 h. After cooling down to room temperature, the resulting mixture was filtered and washed several times with distilled water. Finally, the product was vacuum dried at 60 °C for 24 h, and a brown T-MnO_x powder was obtained.

2.2. Material characterization

The as-prepared powder was characterized by powder X-ray diffraction (XRD) using a D/MAX 2200 VPC X-ray generator in which Cu Kα used as the radiation source. Thermogravimetric analysis (TGA) for the sample was carried out with a STA409PC Diamond TG-DTA thermal analyzer in a nitrogen atmosphere from ambient to 800 °C at a heating rate of 10 °C min^{-1}. The specific surface area and pore size distribution of the sample were analyzed using a surface area analyzer (ASAP-2020, Micromeritics, America), and they were calculated by the Brunauer–Emmett–Teller (BET) equation and the Barrett–Joyner–Halenda (BJH) method, respectively. The microstructure of the sample was obtained from a JSM-6380 scanning electron microscope equipped with energy dispersive X-ray (EDX) spectrometers for the semiquantitative analysis. X-ray photoelectron spectroscopy (XPS) measurements were performed with an ESCALAB 250 X-ray photoelectron spectrometer. Fourier transformation infrared (FT-IR) spectra were recorded using a Fourier transform IR spectrometer (IR-prestige21, Shimadzu Co., Japan) by making pellets with KBr.

2.3. Electrochemical measurements

The working electrode was prepared by mixing 75 wt.% of the as-synthesized T-MnO_x power, 10 wt.% of graphite, 10 wt.% of acetylene black and 5 wt.% of polyvinylidene fluoride (PVDF). A slurry of the above mixture was made using N-methyl-2-pyrrolidone (NMP) as a solvent, then the resulting mixture was coated onto a stainless steel grid with an apparent area of 1 cm × 1 cm and dried under vacuum at 60 °C for 12 h. The electrochemical measurements were carried out using a conventional three-electrode system in which the as-prepared T-MnO_x electrode as the working electrode, graphite electrode as the counter electrode and saturated calomel electrode (SCE) as the reference electrode and 1 M Na_2SO_4 aqueous solution was employed as the electrolyte. Cyclic voltammetry (CV) and galvanostatic charge/discharge (CD) experiments were studied in the potential range from −0.1 to 0.9 V by a CHI 660A electrochemical working station. Electrochemical impedance spectroscopy (EIS) tests were measured using the frequency range from 10^{-2} Hz to 100 kHz by an Autolab PGSTAT30.

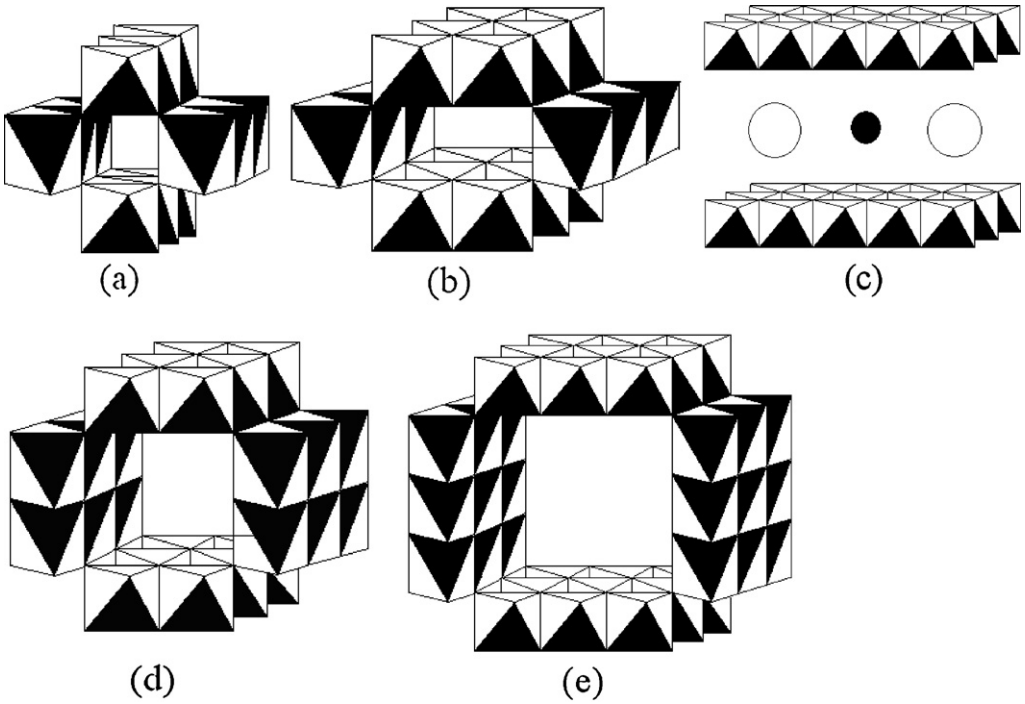

Fig. 1. Tunnel-structure manganese oxides: (a) β-MnO_2, (b) ramsdellite, (c) birnessite, (d) α-MnO_2 and (e) todorokite.

The specific capacitance (SC) of the electrode can be calculated from CV and CD experiments using the following equations, respectively:

$$\mathrm{SC\ (CV)} = \frac{Q}{m\Delta V} \quad (1)$$

$$\mathrm{SC\,(CD)} = \frac{I\Delta t}{m\Delta V} \quad (2)$$

where SC is the specific capacitance ($\mathrm{F\,g^{-1}}$), Q the cathodic charge (C), m the mass of active material in the working electrode (g), ΔV the width of the potential window (V), I the charge or discharge current (A) and Δt is the discharge time (s).

3. Results and discussion

3.1. Characterization of materials

The crystallographic structure of the resultant material was determined by XRD; the XRD data is presented in Fig. 2. Two strong diffraction peaks are observed at $2\theta = 9.3^\circ$ and 18.7° in the XRD pattern. The visibly sharp peaks reveal that the sample is well crystalline. Besides these two main diffraction peaks, another two weak diffraction peaks could be observed at 28.1° and 37.4°. These four diffraction peaks were indexed as the (001), (002), (003) and (004) reflections, respectively, by assuming that the manganese oxide material has a pseudo-orthorhombic cell [18]. All of the diffraction peaks are in good agreement with the standard values of todorokite-type manganese oxide (JCPDS 38-0475) and those reported in a previous study of T-MnO_x [14,15]. The structure of todorokite-type manganese oxide is a 3×3 tunnel structure that belongs to a monoclinic system with a P2/m space group and unit cell parameters of $a = 9.75$ Å, $b = 2.84$ Å, $c = 9.56$ Å and $\beta = 94.07^\circ$ (JCPDS 38-0475). The XRD results show that T-MnO_x was successfully synthesized.

The surface morphology of the synthesized T-MnO_x is shown in Fig. 3. The SEM micrograph clearly shows that the as-synthesized T-MnO_x has an obvious plate-like morphology. The plate-like and fibrous morphologies of T-MnO_x have both been reported in the literature [16,19]. The fragmented platelets of the as-prepared T-MnO_x are irregular in shape and do not aggregate together; the size and thickness of the platelets are approximately 1000 nm and 100 nm, respectively.

The specific surface area and the pore size distribution of the as-prepared sample were studied by nitrogen adsorption–desorption experiments. The BET surface area of the T-MnO_x was calculated to be $14.2\ \mathrm{m^2\,g^{-1}}$, and the corresponding pore volume was approximately $0.02\ \mathrm{cm^3\,g^{-1}}$. BJH analysis further shows that the average pore diameter of the T-MnO_x is approximately 6.5 nm, and the pore size is distributed over the range from 1.8 to 11 nm, indicating the presence of micropores and mesopores in the obtained material according to the International Union of Pure and Applied Chemistry (IUPAC). Although T-MnO_x has a low BET surface area, it exhibits excellent electrochemical capacitive properties. This will be discussed in the following section.

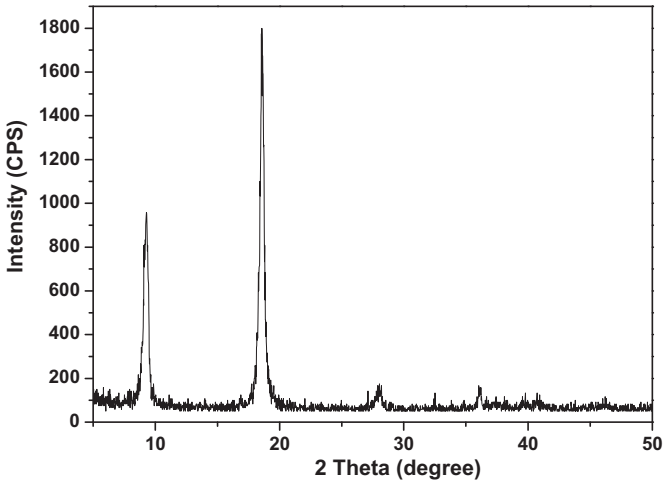

Fig. 2. XRD pattern of the as-prepared T-MnO_x.

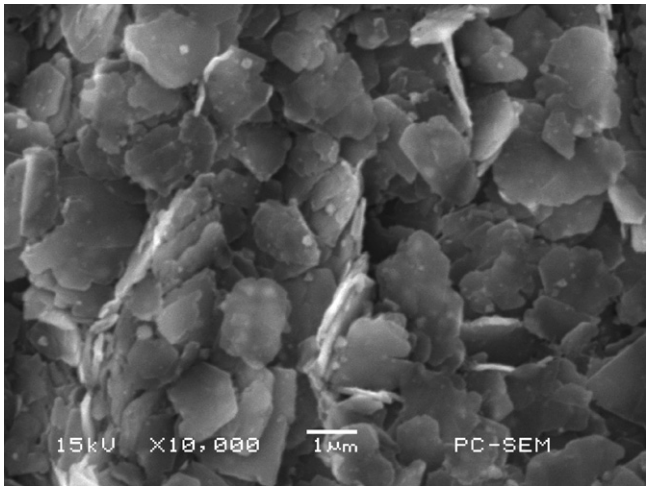

Fig. 3. SEM image of the as-prepared T-MnO_x.

The TGA profile of the T-MnO_x is shown in Fig. 4 for a heating rate of 10 °C min^{-1} from room temperature to 800 °C in a N_2 atmosphere. The total weight loss across the whole temperature range is 24 wt.%. The initially small weight loss of 3.7 wt.% below 200 °C can be mostly attributed to the dehydration of the surface physically adsorbed water. As the temperature increases from 200 °C to around 350 °C, the abrupt and large weight loss should be ascribed to the dehydration of the water bound inside the tunnel [20]. The additional weight loss between 500 and 580 °C is probably due to the reduction of manganese from being tetravalent to trivalent and to the release of generated oxygen from the manganese oxide, resulting in the transformation of T-MnO_x into $MgMn_2O_4$ and Mn_2O_3 [18,20]. From the TGA curve, it can be easily observed that the amount of tunnel water is much higher than that of the physically adsorbed water. Beaudrouet et al. [21] suggested that a certain amount of structural water content can enhance the diffusion of electrolyte cations in the electrode material, which is beneficial to the electrochemical performance of the material.

XPS was employed to study the surface electronic states of the as-prepared material, and the analytical results are shown in Fig. 5. The Mn 2p, Mn 3s, Mg 1s and O 1s XPS spectra of the T-MnO_x are displayed in Fig. 5a, b, c and d, respectively. As shown in the Mn 2p spectrum, the peak appearing at a binding energy of 654.1 eV, which can be assigned to Mn $2p_{1/2}$, indicates that Mn is present in the chemical state of Mn^{4+} [22]. From the shape of the Mn $2P_{3/2}$ spectrum, it can be concluded that a mixture of Mn valence states exists in T-MnO_x. The Mn $2P_{3/2}$ spectrum was deconvoluted into two separate peaks by curve fitting. The peak at a binding energy of 642.6 eV further confirms the existence of Mn^{4+} [23]; the other peak appears at a binding energy of 641.5 eV for Mn $2P_{3/2}$ indicates the presence of the Mn^{3+} chemical state in the sample [24]. According to the literature [25,26], the valence state of Mn can be determined more specifically by investigating the splitting width of two Mn 3s XPS peaks. Fig. 5b shows the XPS spectrum of the Mn 3s orbit of T-MnO_x. The peak separation width (ΔE) of the as-prepared T-MnO_x derived from curve fitting result is 5.08 eV. This value is higher than the reported for MnO_2 of 4.78 eV but lower than Mn_2O_3 of 5.41 eV [25,27]. According to Chigane and Ishikawa [25] and other researchers [27,28], a lower valence of Mn leads to a wider splitting of the Mn 3s peaks. Above analysis result further indicates that trivalent and tetravalent of Mn coexist within the T-MnO_x. Fig. 5c depicts the XPS spectrum of the Mg 1s orbit of T-MnO_x. The broad Mg 1s peak is observed at a binding energy of 1303.3 eV, implying that more than one chemical environment of the Mg atoms exist in the prepared T-MnO_x. The spectrum can be fitted with two peaks at binding energies of 1302.9 eV and 1303.5 eV. According to previous reports [29,30], these two fitted peaks indicate that there are two possible forms of magnesium in the product: free Mg^{2+} ions in the tunnels and the framework incorporation of Mg^{2+} ions in the T-MnO_x material, respectively. The main component at a higher binding energy is typical for Mg^{2+} ions in the framework of the T-MnO_x for structural stability. The other relatively small peak at a lower binding energy can be attributed to Mg^{2+} ions in the tunnel, which is in a more reduced state and can be easily substituted by other cations; thus, the relative number of Mg^{2+} ions in the T-MnO_x tunnel may decrease in the ensuing electrochemical measurements. The O 1s spectrum of the T-MnO_x was analyzed by curve fitting as shown in Fig. 5d. The spectrum can be deconvoluted into two sharp peaks and one broad peak, which correspond to three different oxygen-containing species: the anhydrous manganese oxide (Mn–O–Mn) at 530.1 eV, the hydrated manganese (Mn–O–H) at 531.3 eV and the water molecule (H–O–H) at 532.4 eV, which are in good agreement with the reported values of 529.3–530.3 eV for Mn–O–Mn, 530.5-531.5 eV for Mn–O–H and 531.8–532.8 eV for H–O–H, respectively [28]. Moreover, it is also found that T-MnO_x contains a relatively large amount of hydrated manganese, which is in good agreement with the TGA result.

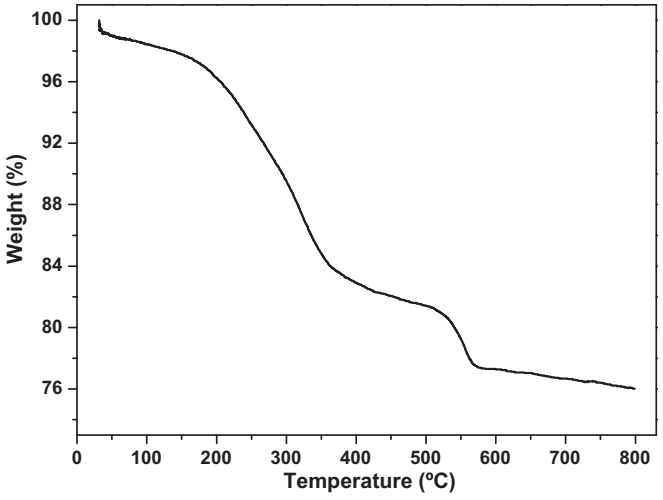

Fig. 4. TGA curve of the as-prepared T-MnO_x.

3.2. Electrochemical properties

The CV technique was employed to investigate the supercapacitive properties of the as-prepared T-MnO_x. The first-cycle CV curve of the T-MnO_x electrode is presented in Fig. 6a. The CV curve was recorded in 1 M Na_2SO_4 electrolyte within the potential range of −0.1 to 0.9 V versus SCE at a scan rate of 5 mV s^{-1}. It can be observed that the CV curve exhibits a roughly rectangular shape and no obvious redox peak in the potential range between −0.1 and 0.9 V. The specific capacitance calculated from the first-cycle CV curve according to Eq. (1) is found to be 94 F g^{-1}.

The long-term cycling stability of the as-prepared T-MnO_x was investigated by long CV cycles up to 23,000 cycles at a scan rate of 50 mV s^{-1}. To understand the capacitance variation during the CV cycles, the initial specific capacitance was set to 100%, and the variation of the capacitance retention ratio as a function of cycle number is shown in Fig. 7. The specific capacitance of the sample rapidly increases during the initial 1000 cycles and then improves gradually; it finally reaches a maximum (170% vs. the initial value) at approximately 4000th-cycle. Such an improvement in the specific capacitance during a number of initial cycles was also reported in

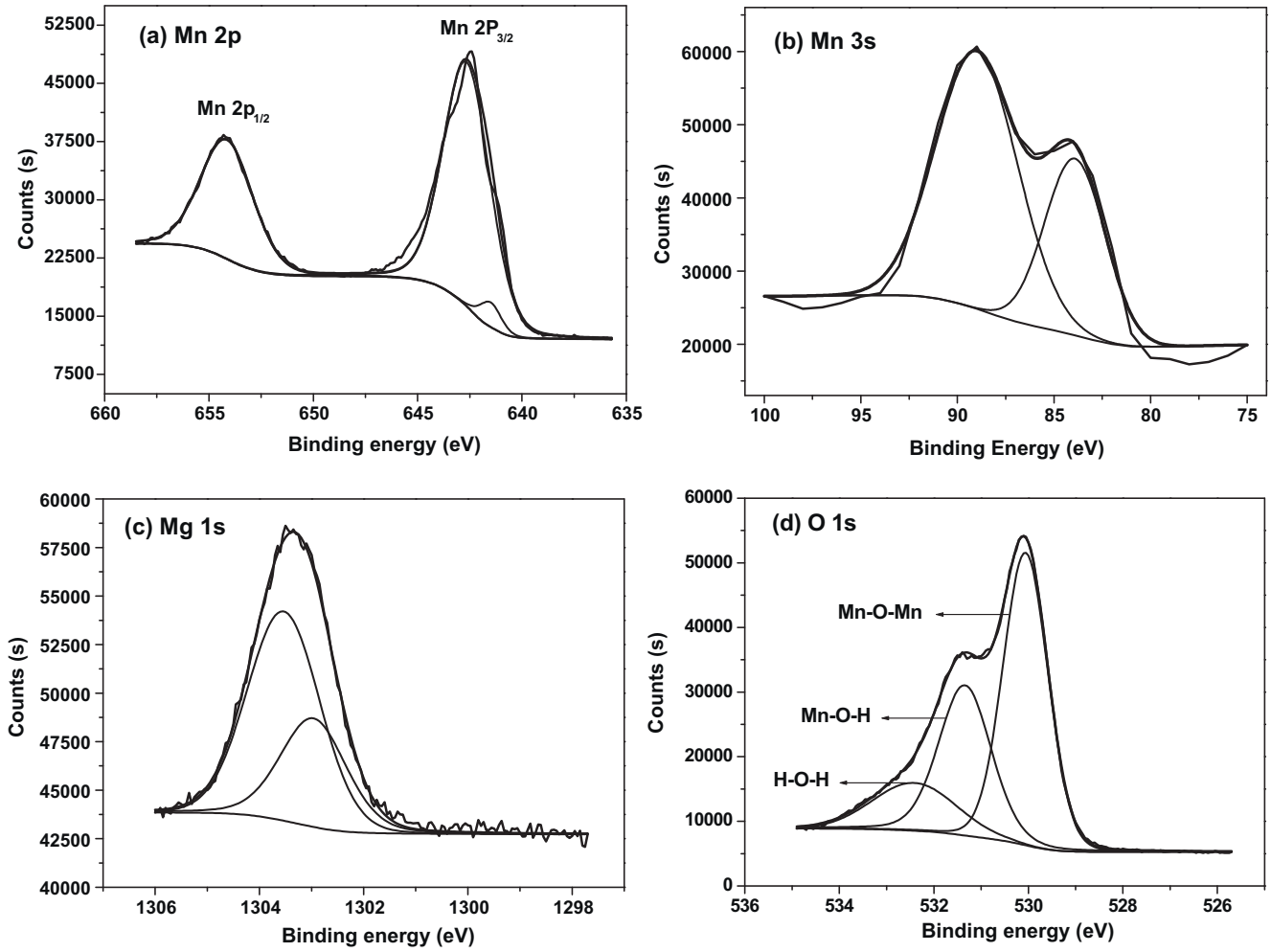

Fig. 5. XPS spectra of the T-MnO_x: (a) Mn 2p peak, (b) Mn 3s peak, (c) Mg 1s peak and (d) O 1s peak.

previous studies on manganese oxides [23,31]. Thereafter, the specific capacitance remains almost constant and decreases slightly upon prolonged cycling. After 23,000 cycles, the specific capacitance value remains approximately 160% of the initial capacitance value and decreases by 6% of the maximum specific capacitance. It is concluded that the as-prepared material presents excellent overall long-term stability, which suggests that T-MnO_x is a promising electrode material for supercapacitor applications.

According to the above analysis, it can be concluded that the specific capacitance reaches a maximum after 4000 cycles. Thus, further experiments were performed on the T-MnO_x electrode after 4000 cycles.

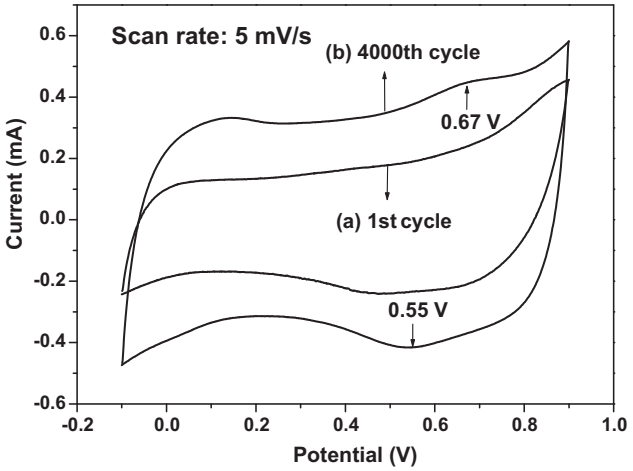

Fig. 6. Cyclic voltammograms of the T-MnO_x electrode at different cycles at a scan rate of 5 mV s^{-1}.

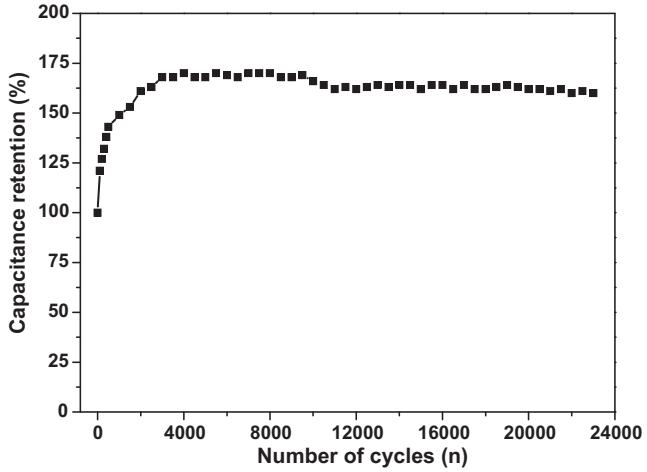

Fig. 7. Variation of capacitance retention (%) with respect to cycle number at scan rate of 50 mV s^{-1}.

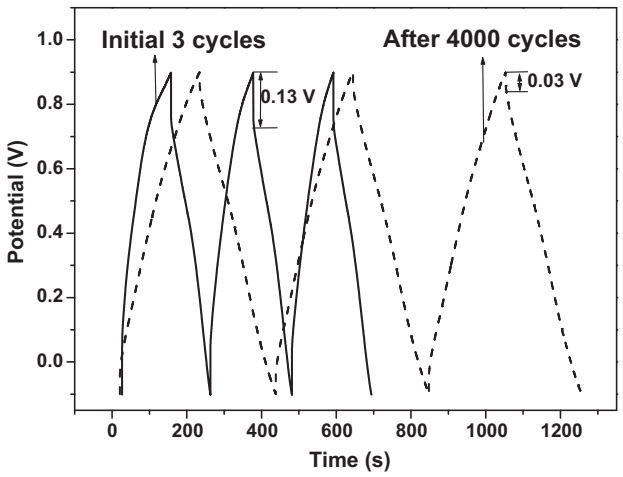

Fig. 8. The charge–discharge curves of the initial 3 cycles and after 4000 cycles for the T-MnO_x electrode at a current density of 1 A g^{-1}.

Fig. 6b also shows the 4000th-cycle CV curve at a scan rate of 5 mV s^{-1}. The enclosed area for the 4000th-cycle CV curve is apparently larger than that of the first cycle, indicating an enhancement in the specific capacitance. The specific capacitance calculated from the 4000th-cycle CV curve is 189 F g^{-1}, which is much larger than the value 94 F g^{-1} observed for the first cycle. In addition, a pair of symmetric redox peaks is observed in the CV curve of the 4000th cycle, and the broad anodic and cathodic peaks are located at 0.67 and 0.55 V versus SCE, respectively. This behavior suggests that faradic phenomena occur during the charge-storage mechanism.

The supercapacitive behavior of T-MnO_x was also measured by CD testing. Fig. 8 depicts the typical charge–discharge curves of the initial 3 cycles and after 4000 cycles for the T-MnO_x electrode at a current density of 1 A g^{-1} in 1 M Na_2SO_4 electrolyte between −0.1 and 0.9 V versus SCE. The charge–discharge curves after 4000 cycles are almost similar to the initial cycles, except for the fact that they exhibit a smaller initial potential drop, indicating that the polarization resistance of the material becomes smaller during electrochemical cycling. In general, the small initial potential drop leads to a large specific capacitance [32]. Thus, after 4000 cycles, the charge–discharge time becomes much longer than that of the initial cycles, indicating that the specific capacitance of the T-MnO_x electrode increases during the cycling process. The specific capacitance after 4000 cycles was calculated according to Eq. (2) is 209 F g^{-1}.

The electrochemical behavior of the T-MnO_x electrode after 4000 cycles was further characterized by CV at different scan rates ranging from 2 to 100 mV s^{-1}. An analysis of the scan-rate dependence can provide useful information concerning charge storage in the electrode material. Fig. 9a depicts CV curves of the T-MnO_x electrode after 4000 cycles at different scan rates. It can be observed that the CV curves of the sample are relatively rectangular and symmetric at low scan rates. With an increase in the scan rate, the CV curves gradually change from being rectangular in shape to being

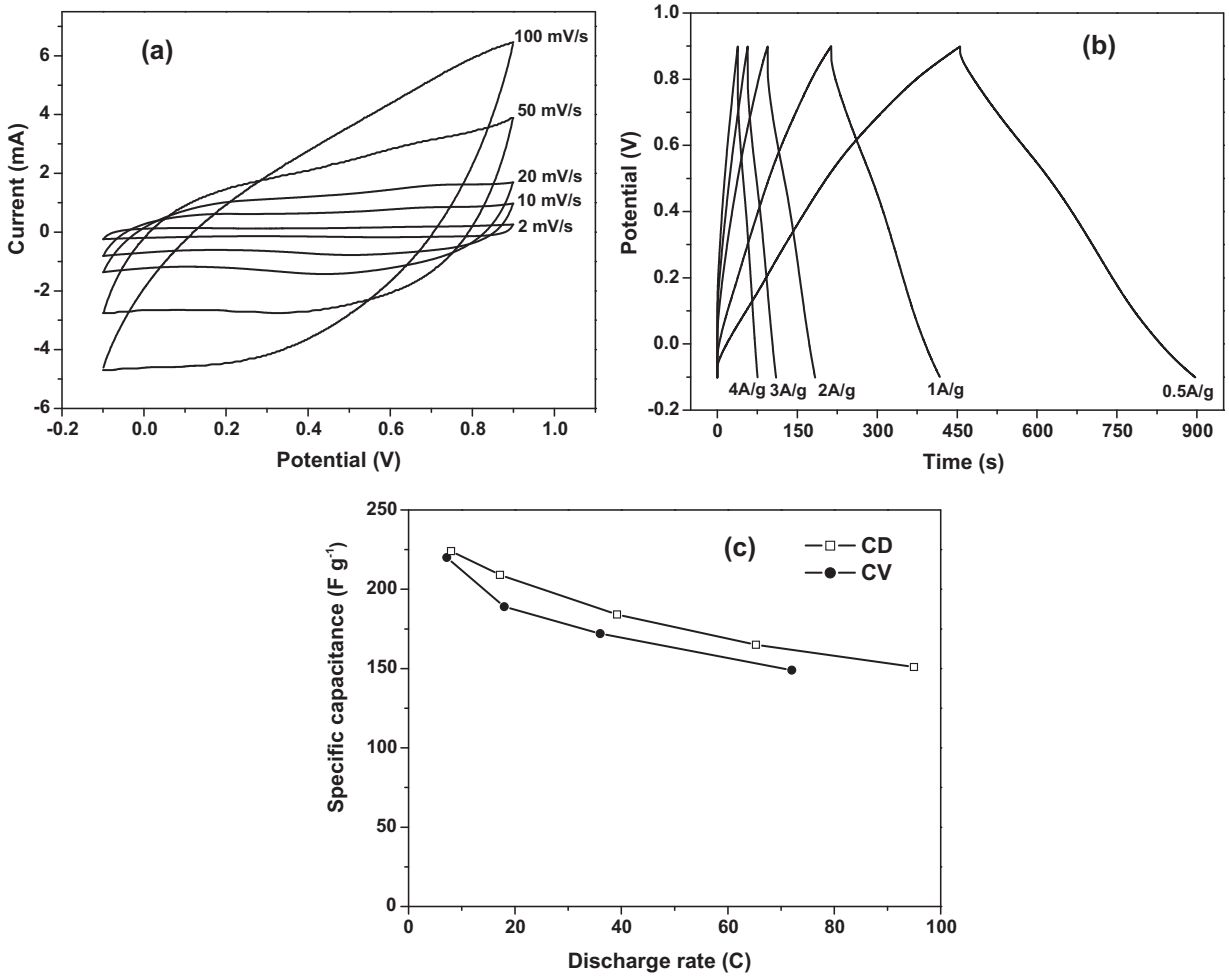

Fig. 9. (a) Cyclic voltammograms at various scan rates and (b) charge–discharge curves at different current densities for the T-MnO_x electrode after 4000 cycles and (c) the corresponding specific capacitance as a function of discharge rate.

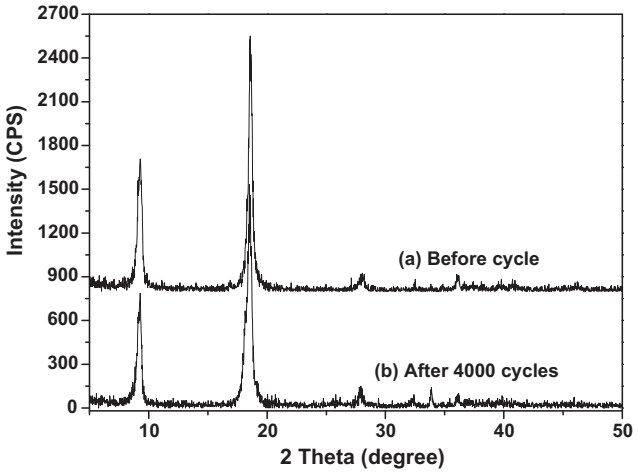

Fig. 10. XRD patterns of the as-prepared T-MnO_x: (a) before and (b) after 4000 cycles.

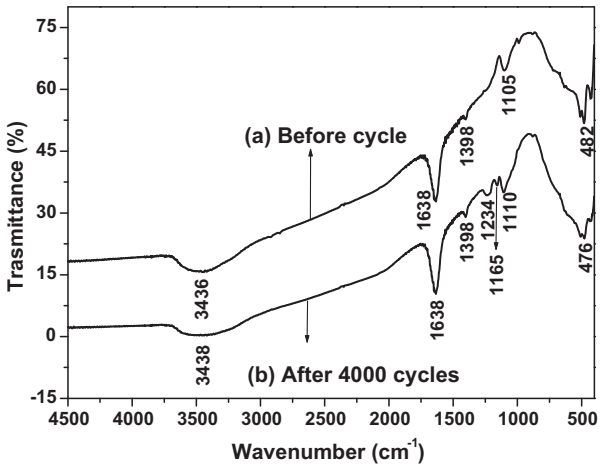

Fig. 11. FT-IR spectra of the T-MnO_x: (a) before and (b) after 4000 cycles.

shuttle-shaped. The specific capacitance was calculated from the above CV curves, and the result shows that the specific capacitance values quickly decrease from 220 to 67 F g^{-1} as the scan rates increases from 2 to 100 mV s^{-1}. It has been reported [7,33,34] that the scan rate has a direct effect on the diffusion of Na^+ ions. At low scan rates, such as 2 mV s^{-1}, Na^+ ions can access almost all available pores of the electrode, leading to nearly full utilization of the surface and bulk of the electrode material. Therefore, the system shows almost ideal capacitive behavior. However, at higher scan rates, Na^+ ions do not have enough time to diffuse into the whole volume of the T-MnO_x electrode; consequently, some pores and voids remain inaccessible, so the specific capacitance decreases appreciably.

Further CD measurements were also carried out in 1 M Na_2SO_4 at different current densities to obtain more information about the supercapacitive behavior of the T-MnO_x electrode after 4000 cycles. As shown in Fig. 9b, the straight line characteristic in the charge and discharge curves implies the excellent capacitive nature of the active material. The average specific capacitances calculated from the charge–discharge curves at current densities of 0.5, 1, 2, 3 and 4 A g^{-1} are 224, 209, 184, 165 and 151 F g^{-1}, respectively. The specific capacitance clearly decreases when the charge–discharge current density increases, showing the same tendency as that reported in the above CV studies.

To compare the specific capacitance values obtained by CV experiments with those calculated from CD tests, the scan rate in the CV experiments and the discharge time in the CD tests were converted to a discharge rate. The specific capacitance values of the T-MnO_x electrode after 4000 cycles (calculated from the CV and CD tests) versus the discharge rate are shown in Fig. 9c. It can be easily observed that the specific capacitance calculated from the CD tests are close to but slightly larger than those obtained by CV experiments at the same discharge rate. The results suggest that the specific capacitance values calculated from CV and CD tests can be compared at the same discharge rate.

To understand the structural stability of the T-MnO_x during electrochemical cycling, the XRD pattern of the T-MnO_x was recorded after 4000 CV cycles and shown in Fig. 10. To avoid the interference by the diffraction peak of graphite and further compare the structure change of the pure T-MnO_x during electrochemical cycle, the working electrode was specially prepared by mixing 85 wt.% of the as-synthesized T-MnO_x power, 10 wt.% of acetylene black and 5 wt.% of PVDF for XRD measurement. The typical diffraction peaks of the T-MnO_x, such as those at $2\theta = 9.3^\circ$, 18.7°, 28.1° and 37.4°, still remain in Fig. 10b. Because of higher content and stronger diffraction peaks of T-MnO_x and the smaller amount and weaker diffraction peaks of acetylene black and PVDF, the diffraction peaks of acetylene black and PVDF are not clearly observed in the XRD patterns of the T-MnO_x electrode after 4000 electrochemical cycles. This XRD result reflects that long-term electrochemical cycling does not induce significant structural modifications of the T-MnO_x electrode. Therefore, the increase in the specific capacitance for the T-MnO_x electrode during thousands of initial electrochemical cycles is attributed to a gradual electrochemical activation process.

To understand the differences in the chemical bonds in T-MnO_x between before and after 4000 cycles, FT-IR analysis was carried out in the wavelength range from 450 to 4500 cm^{-1}, and the resulting FT-IR spectra are shown in Fig. 11. It can be observed that the FT-IR spectrum of the T-MnO_x before electrochemical measurement (Fig. 11a) is similar to that of the sample after 4000 cycles (Fig. 11b). The two spectra show the same broad band at around 3436 cm^{-1} due to the O–H stretching vibrations of adsorbed water molecules or hydroxyl groups [35]; the absorption peaks at around 1638, 1398 and 1105 cm^{-1} can be assigned to the O–H bending vibrations combined with Mn atoms [36], and the Mn–O stretching vibrations in MnO_6 octahedra framework can be observed at approximately 513, 476 and 427 cm^{-1} [37]. However, two new weak absorption peaks appear at around 1234 and 1165 cm^{-1} after 4000 cycles, which are normally attributed to the O–H bending vibrations connected to Mn atoms. Some experts believe that the presence of bound water in the manganese oxide structure facilitates the diffusion of Na^+ ions in the bulk of the electrode, which produces favorable electrochemical properties for manganese oxide as an electrode material for supercapacitors [36,38]. The FT-IR results are in good agreement with the above XRD analysis data, and both demonstrate the excellent structural stability of the T-MnO_x electrode during electrochemical cycling.

The fresh T-MnO_x electrode and the T-MnO_x electrode after 4000 cycles were also studied by SEM at the same magnification; the SEM images are shown in Fig. 12a and b. The T-MnO_x was observed to possess plate-like morphology in Fig. 12b, indicating that the morphology of the T-MnO_x is retained even after 4000 cycles. A better understanding of the electrochemical behavior of the T-MnO_x electrode was obtained by EDX measurements. The Na/Mn and Mg/Mn atomic ratios of the T-MnO_x electrode before and after 4000 CV cycles in 1 M Na_2SO_4 electrolyte are shown in Fig. 12c. Fig. 12c shows that the Mg/Mn atomic ratio decreases from 0.21 to 0.16 after thousands of cycles, indicating that some Mg^{2+} ions dissolve from the electrode during cycling. The Na/Mn atomic ratio of the fresh T-MnO_x electrode is approximately 0.01, the slight amount of Na^+ ions is mainly due to the residual Na^+ ions that remain after repeated cleaning during synthesis, though

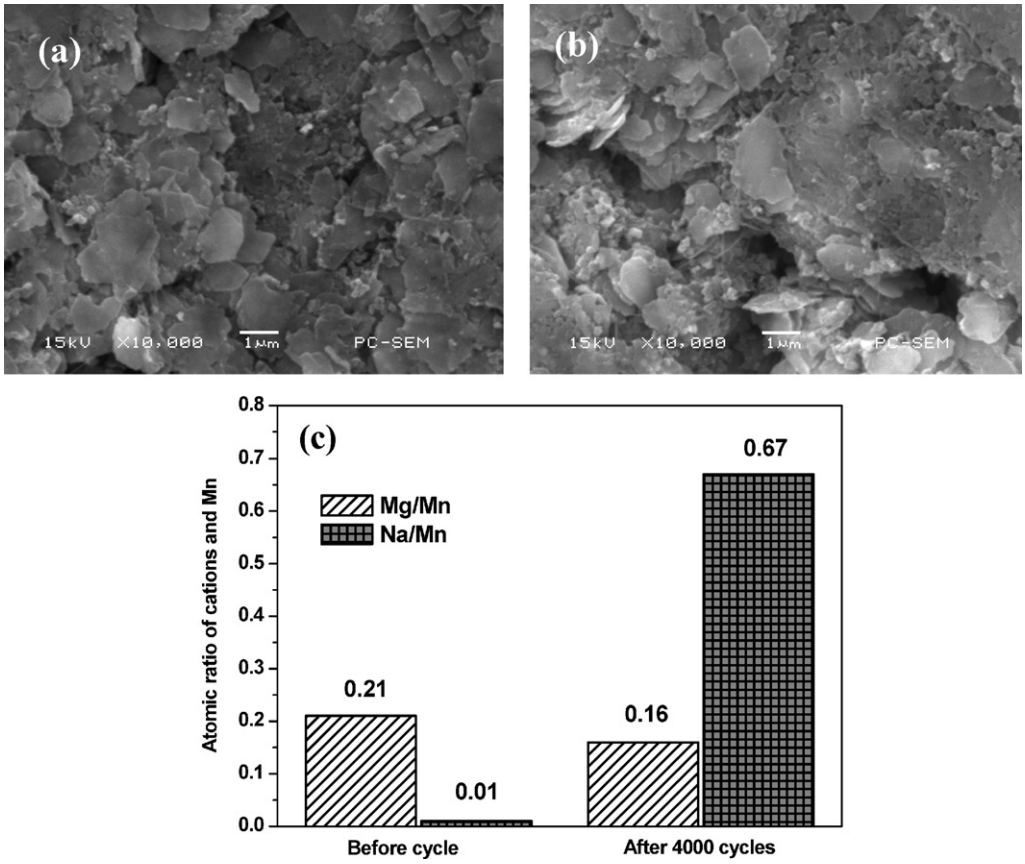

Fig. 12. (a) SEM images of the working electrode was prepared by using the acquired T-MnO_x as active material before cycle and (b) after 4000 cycles. (c)The Na/Mn and Mg/Mn atomic ratios of the T-MnO_x obtained from EDX studies before and after 4000 cycles.

the Na/Mn atomic ratio reaches 0.67 after 4000 cycles. According to the literature [11], Mg^{2+} and Na^+ ions exist in T-MnO_x to compensate the negative charges on the MnO_2 framework. Based on the atomic ratio data in Fig. 12c, the total positive charge of Mg^{2+} and Na^+ is $0.43(0.21 \times 2 + 0.01)$ for the fresh T-MnO_x electrode, indicating the oxidation number of Mn is 3.57. This result is consistent with the above XPS results, which demonstrate the presence of the Mn^{4+} and Mn^{3+} chemical state in T-MnO_x. In the cycling experiment, the cycle was stopped in the reduced state at a potential of −0.1 V versus SCE. The total positive charge of Mg^{2+} and Na^+ is $0.99(0.16 \times 2 + 0.67)$ for the T-MnO_x after 4000 cycles, corresponding to the oxidation number of Mn is 3.01. The higher Na/Mn atomic ratio and lower oxidation number of Mn is consistent with charge compensation by Na^+ ions from the electrolyte at the reduced state, which was reported by Athouel et al. [11] and Toupin et al. [39]. According to the in situ XRD experiment [40,41], the intercalation/deintercalation compound can reserve its structure stability during various oxidation state.

According to the above XPS analysis result, two possible forms of Mg^{2+} ions exist in the sample: free Mg^{2+} ions in the tunnels and the framework-incorporated Mg^{2+} ions in the T-MnO_x material. The results of the above XRD and FT-IR analysis demonstrate the excellent structural stability of the T-MnO_x during electrochemical cycling, which indicates that the Mg^{2+} ions in the framework should be retained in the T-MnO_x structure and support the structural stability. Therefore, the Mg^{2+} ions in the tunnel deintercalate gradually and undergo ion exchange with Na^+ ions in the electrolyte solution during the initial electrochemical cycles. Moreover, with its large tunnel structure, T-MnO_x can accommodate many more Na^+ ions, which provide additional specific capacitance. Such an activation process during thousands of initial electrochemical cycles results in a gradual increase in the specific capacitance of the T-MnO_x electrode.

According to previous studies, two mechanisms were proposed to explain the supercapacitive behavior of MnO_2 in a mild solution. The first is the surface adsorption of electrolyte cations ($C^+ = H^+$, Li^+, Na^+ or K^+) on the manganese oxides [6].

$$(MnO_2)_{surface} + C^+ + e^- \leftrightarrow (MnO_2{}^-C^+)_{surface} \quad (3)$$

The second is based on the intercalation or deintercalation of electrolyte cations ($C^+ = H^+$, Li^+, Na^+ or K^+) in the bulk of the manganese oxides during reduction [39].

$$MnO_2 + C^+ + e^- \leftrightarrow MnOOC^+ \quad (4)$$

In our present study, the specific capacitance increases during electrochemical cycles before 4000 cycles. This is attributed to the gradual activation process of the T-MnO_x electrode. During initial electrochemical cycles, Mg^{2+} ions in the tunnel of the T-MnO_x hinder Na^+ ions from electrolyte diffusion into the tunnels, resulting in a low specific capacitance value. Along with the cycling, the electrolyte gradually soaks into the bulk of the electrode, and Mg^{2+} ions in the tunnel of the T-MnO_x deintercalate from the electrode, which facilitates Na^+ ions diffusion into the tunnels. According to equation 4, Na^+ ions reversibly intercalate/deintercalate into the T-MnO_x electrode, providing a considerable pseudocapacitive contribution. Thus, the electrode exhibits excellent capacitance behavior after 4000 cycles. The specific capacitance of the T-MnO_x electrode remains an almost constant value until 23,000 cycles with the increase in cycle number, which indicates that the intercalation and deintercalation of Na^+ ions into the tunnel of the T-MnO_x do not result in significant structural or microstructural changes of the T-MnO_x, even after 23000 cycles.

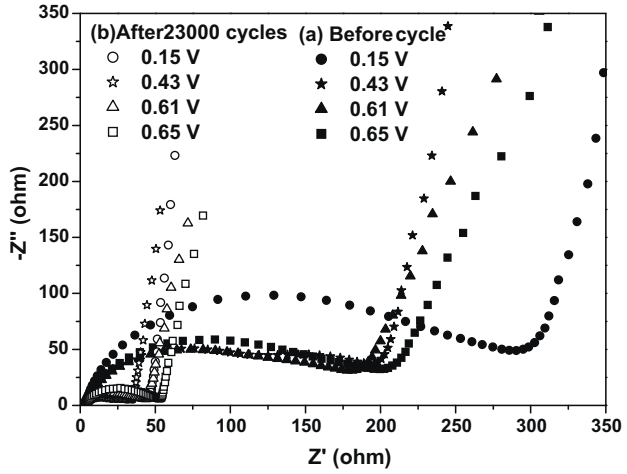

Fig. 13. Nyquist plots of the T-MnO_x electrode in the frequency range of 10^{-2} Hz to 100 kHz: (a) before and (b) after 23,000 cycles.

Nyquist plots of the T-MnO_x electrode before and after electrochemical measurements in 1 M Na_2SO_4 electrolyte at different potentials are shown in Fig. 13. It can be clearly observed that all of the measured impedance plots are similar in shape. At very high frequencies, the EIS curves exhibit almost the same combined resistance of the ionic resistance of the electrolyte, the intrinsic resistance of the T-MnO_x electrode and the contact resistance at the interface between the T-MnO_x electrode and the current collector. The semicircle in the high-frequency range is usually associated with the electrochemical processes of the T-MnO_x electrode, and the diameter of the semicircle corresponds to the charge-transfer resistance (R_{ct}). It can be easily observed from Fig. 13 that the diameters of the semicircles clearly decrease after 4000 cycles. Variations in the R_{ct} of the T-MnO_x electrode in different cycles with potential are shown in Fig. 14. Compared with the fresh electrode, all of the R_{ct} of the T-MnO_x electrode after 4000 and 23,000 cycles at various potentials are reduced, but they are close to each other at the same potential. It can be concluded that the initial thousands of cycles provide an electrochemical activation process, which leads to the decrease in the charge-transfer resistance and the increase in the specific capacitance. At lower frequencies, the straight sloping lines along the imaginary axis represent the diffusive resistance of the electrolyte in the electrode pores and the proton diffusion in the host material. All of the plots of the T-MnO_x electrode are almost perpendicular to the real axis, indicating that the material has low diffusive resistance and ideal capacitance. A comparison of Fig. 13a and b reveals that the slopes of the diffusion lines become much straighter after 23,000 cycles for all potentials, which indicates that the diffusive resistance apparently decreases during cycling. We believe that the specific capacitance is significantly influenced by the diffusive resistance and R_{ct}, so the electrochemical capacitive properties of the T-MnO_x electrode improve significantly during the initial thousands of cycles.

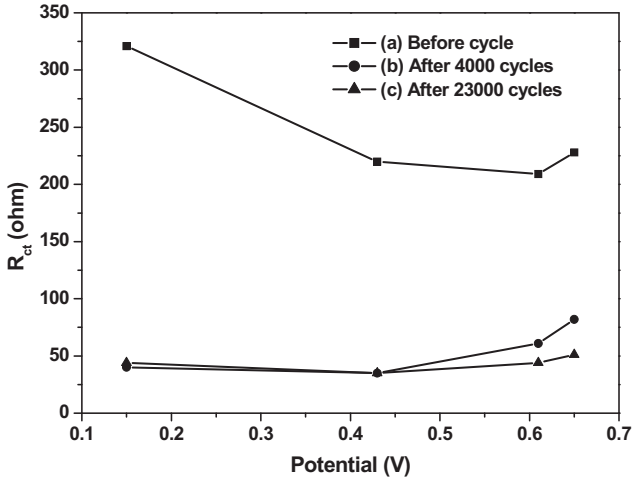

Fig. 14. The charge-transfer resistance (R_{ct}) at different potentials calculated from the above electrochemical impedance spectra.

4. Conclusions

In this paper, T-MnO_x with a 3×3 large tunnel structure was successfully prepared using a hydrothermal method. The supercapacitive behaviors of the obtained material were studied by CV, CD and EIS experiments. The results show that the specific capacitance of the T-MnO_x electrode sharply increases during the initial 1000 cycles and then continues to gradually improve; it reaches a maximum of 220 F g^{-1} at approximately the 4000th cycle at the scan rate of 2 mV s^{-1}. Thereafter, the specific capacitance remains almost constant and decreases slightly upon prolonged cycling. After 23,000 cycles, it decreases by 6% of the maximum specific capacitance. Further XRD and FT-IR analyses revealed retention of the structural stability of T-MnO_x during electrochemical cycling. Thus, the increase in the specific capacitance of the T-MnO_x electrode during the initial thousands of cycles is attributed to an electrochemical activation process. During the initial electrochemical cycles, the Mg^{2+} ions in the framework are preserved in the T-MnO_x structure and support the structural stability; the Mg^{2+} ions in the tunnel of the T-MnO_x hinder Na^+ ions from diffusing from the electrolyte into tunnels, resulting in a low specific capacitance. During electrochemical cycling, the Mg^{2+} ions in the tunnel of the T-MnO_x deintercalate from electrode, which facilitates Na^+ ion diffusion into the tunnels, Moreover, the large tunnel of the T-MnO_x can accommodate many more Na^+ ions, allowing for a higher specific capacitance. In addition, the charge-transfer resistance (R_{ct}) of the T-MnO_x electrode apparently decreases after 4000 cycles and then remains at almost a constant value up to 23,000 cycles. The excellent supercapacitive performances of the as-prepared T-MnO_x suggest its potential application as a supercapacitor electrode material.

Acknowledgements

The authors wish to acknowledge the financial support for this work from Guangdong Province Sci. & Tech. Bureau (Grant No. 2010B090400552), Natural Science Foundation of Guangdong Province, China (Grant No. S2011010003416), China High-Tech Development 863 Program (Grant No. 2009AA03Z340) and National Natural Science Foundation of China (Grant No. 20877025).

References

[1] B.E. Conway, Electrochemical Supercapacitors, Scientific Fundamentals and Technological Applications, Kluwer Academic/Plenum Press, New York, 1999.
[2] L.L. Zhang, X.S. Zhao, Chem. Soc. Rev. 38 (2009) 2520–2531.
[3] Y. Hou, Y.W. Cheng, T. Hobson, J. Liu, Nano Lett. 10 (2010) 2727–2733.
[4] H. Li, J. Wang, Q. Chu, Z. Wang, F. Zhang, S. Wang, J. Power Sources 190 (2009) 578–586.
[5] J.P. Zheng, T.R. Jow, J. Power Sources 62 (1996) 155–159.
[6] H.Y. Lee, J.B. Goodenough, J. Solid State Chem. 144 (1999) 220–223.
[7] M. Toupin, T. Brousse, D. Belanger, Chem. Mater. 14 (2002) 3946–3952.
[8] T. Brousse, M. Toupin, R. Dugas, L. Athouel, O. Crosnier, D. Belanger, J. Electrochem. Soc. 153 (2006) A2171–A2180.
[9] O. Ghodbane, J.L. Pascal, F. Favier, ACS Appl. Mater. Interfaces 1 (2009) 1130–1139.
[10] D.J. Jones, E. Wortham, J. Roziere, F. Favier, J.L. Pascal, L. Monconduit, J. Phys. Chem. Solids 65 (2004) 235–239.

[11] L. Athouel, F. Moser, R. Dugas, O. Crosnier, D. Belanger, T. Brousse, J. Phys. Chem. C 112 (2008) 7270–7277.
[12] X.Y. Wang, X.Y. Wang, W.G. Huang, P.J. Sebastian, S. Gambao, J. Power Sources 140 (2005) 211–215.
[13] S. Devaraj, N. Munichandraiah, J. Phys. Chem. C 112 (2008) 4406–4417.
[14] Y. Yang, D. Shu, H. Yu, X. Xia, Z.G. Lin, J. Power Sources 65 (1997) 227–230.
[15] Y. Yang, D. Shu, H. Yu, J.K. Yon, Z.G. Lin, J. Power Sources 81-82 (1999) 637–641.
[16] A. Onda, S. Hara, K. Kajiyoshi, K. Yanagisawa, Appl. Catal. A: Gen. 321 (2007) 71–78.
[17] S. Ching, K.S. Krukowska, S.L. Suib, Inorg. Chim. Acta 294 (1999) 123–132.
[18] Y.F. Shen, R.P. Zerger, R.N. Deguzman, S.L. Suib, L. Mccurdy, D.I. Potter, C.L. O'Young, Science 260 (1993) 511–515.
[19] Z.H. Liu, L.P. Kang, K. Ooi, Y. Makita, Q. Feng, J. Colloid Interface Sci. 285 (2005) 239–246.
[20] Y.F. Shen, S.L. Suib, C.L. O'Young, J. Am. Chem. Soc. 116 (1994) 11020–11029.
[21] E. Beaudrouet, A.L.G. La Salle, D. Guyomard, Electrochim. Acta 54 (2009) 1240–1248.
[22] S.L. Chou, F.Y. Cheng, J. Chen, J. Power Sources 162 (2006) 727–734.
[23] Z.P. Feng, G.R. Li, J.H. Zhong, Z.L. Wang, Y.N. Ou, Y.X. Tong, Electrochem. Commun. 11 (2009) 706–710.
[24] B.R. Strohmeier, D.M. Hercules, J. Phys. Chem. 88 (1984) 4922–4929.
[25] M. Chigane, M. Ishikawa, J. Electrochem. Soc. 147 (2000) 2246–2251.
[26] M. Chigane, M. Ishikawa, M. Izaki, J. Electrochem. Soc. 148 (2001) D96–D101.
[27] M. Nakayama, A. Tanaka, Y. Sato, T. Tonosaki, K. Ogura, Langmuir 21 (2005) 5907–5913.
[28] B. Djurfors, J.N. Broughton, M.J. Brett, D.G. Ivey, Acta Mater. 53 (2005) 957–965.
[29] E. Nicolas-Tolentino, Z.R. Tian, H. Zhou, G.G. Xia, S.L. Suib, Chem. Mater. 11 (1999) 1733–1741.
[30] W.N. Li, J.K. Yuan, X.F. Shen, S. Gomez-Mower, L.P. Xu, Adv. Funct. Mater. 16 (2006) 1247–1253.
[31] J.Q. Yuan, Z.H. Liu, S.F. Qiao, X.R. Ma, N.C. Xu, J. Power Sources 189 (2009) 1278–1283.
[32] X. Du, C.Y. Wang, M.M. Chen, Y. Jiao, J. Wang, J. Phys. Chem. C 113 (2009) 2643–2646.
[33] M.W. Xu, L.B. Kong, W.J. Zhou, H.L. Li, J. Phys. Chem. C 111 (2007) 19141–19147.
[34] X.H. Yang, Y.G. Wang, H.M. Xiong, Y.Y. Xia, Electrochim. Acta 53 (2007) 752–757.
[35] Z. Liu, X. Yang, Y. Makita, K. Ooi, Chem. Mater. 14 (2002) 4800–4806.
[36] X.L. Wang, A.B. Yuan, Y.Q. Wang, J. Power Sources 172 (2007) 1007–1011.
[37] T. Gao, M. Glerup, F. Krumeich, R. Nesper, H. Fjellvag, P. Norby, J. Phys. Chem. C 112 (2008) 13134–13140.
[38] P. Ragupathy, D.H. Park, G. Campet, H.N. Vasan, S.J. Hwang, J.H. Choy, N. Munichandraiah, J. Phys. Chem. C 113 (2009) 6303–6309.
[39] M. Toupin, T. Brousse, D. Belanger, Chem. Mater. 16 (2004) 3184–3190.
[40] G.X. Wang, Z.P. Guo, X.Q. Yang, J. McBreen, H.K. Liu, S.X. Dou, Solid State Ionics 167 (2004) 183–189.
[41] X.Q. Yang, X. Sun, S.J. Lee, J. McBreen, S. Mukerjee, M.L. Daroux, X.K. Xing, Electrochem. Solid-State Lett. 2 (1999) 157–160.